Stem Cell Reports
Article

ISSCR

OPEN ACCESS

The Snakeskin-Mesh Complex of Smooth Septate Junction Restricts Yorkie to Regulate Intestinal Homeostasis in *Drosophila*

Hsi-Ju Chen,[1] Qi Li,[1] Niraj K. Nirala,[1] and Y. Tony Ip[1,*]
[1]Program in Molecular Medicine, University of Massachusetts Medical School, Worcester, MA 01605, USA
*Correspondence: tony.ip@umassmed.edu
https://doi.org/10.1016/j.stemcr.2020.03.021

SUMMARY

Tight junctions in mammals and septate junctions in insects are essential for epithelial integrity. We show here that, in the *Drosophila* intestine, smooth septate junction proteins provide barrier and signaling functions. During an RNAi screen for genes that regulate adult midgut tissue growth, we found that loss of two smooth septate junction components, Snakeskin and Mesh, caused a hyperproliferation phenotype. By examining epitope-tagged endogenous Snakeskin and Mesh, we demonstrate that the two proteins are present in the cytoplasm of differentiating enteroblasts and in cytoplasm and septate junctions of mature enterocytes. In both enteroblasts and enterocytes, loss of Snakeskin and Mesh causes Yorkie-dependent expression of the JAK-STAT pathway ligand Upd3, which in turn promotes proliferation of intestinal stem cells. Snakeskin and Mesh form a complex with each other, with other septate junction proteins and with Yorkie. Therefore, the Snakeskin-Mesh complex has both barrier and signaling function to maintain stem cell-mediated tissue homeostasis.

INTRODUCTION

The balance between self-renewal of stem cells and differentiation of progeny cells has to be maintained precisely, or otherwise may lead to tumor growth or tissue degeneration (Clevers et al., 2014; Qin and Zhang, 2017). The adult *Drosophila* midgut is a highly useful genetic model system to dissect intestinal stem cell (ISC)-mediated homeostasis (Herrera and Bach, 2019; Micchelli and Perrimon, 2006; Ohlstein and Spradling, 2006; Zwick et al., 2019). Approximately a thousand ISCs are evenly distributed throughout the adult *Drosophila* midgut epithelium (Micchelli and Perrimon, 2006; Ohlstein and Spradling, 2006). An ISC undergoes asymmetric division to generate a renewed ISC and another daughter cell called enteroblast (EB) or pre-enteroendocrine cell (pre-EE), which can differentiate to become an enterocyte (EC) for absorption or an EE for hormone production, respectively (Figure 1A) (Chen et al., 2018; Ohlstein and Spradling, 2007; Zeng and Hou, 2015). Many conserved pathways, including Delta-Notch, Insulin, JAK-STAT, BMP, and Wnt are used to control ISC asymmetry, division rate, and subsequent differentiation along the two lineages (Amcheslavsky et al., 2009; Biteau and Jasper, 2011; Chen et al., 2018; Cordero et al., 2012; Guo and Ohlstein, 2015; Jiang et al., 2009; Ohlstein and Spradling, 2007; Tian and Jiang, 2014; Xu et al., 2011; Zeng and Hou, 2015).

We and others recently have shown that the Ste20 kinases Misshapen (Msn) and Happyhour (Hppy) functions similar to Hippo (Hpo) to regulate the Warts-Yorkie (Wts-Yki) axis (Karpowicz et al., 2010; Li et al., 2014, 2015, 2018; Meng et al., 2015; Ren et al., 2010; Shaw et al., 2010; Staley and Irvine, 2010; Zheng et al., 2015). In adult *Drosophila* midgut, Msn is expressed rather specifically in ISCs/EBs (Li et al., 2018). The function of Msn in EBs is modulated by ingested solid food particles that change the mechanical stretching of the midgut epithelium, and leads to regulation of Yki and Unpaired3 (Upd3) to control ISC division and tissue growth (Li et al., 2018). Hpo has a possible parallel mechanosensing function in ECs after epithelial damage (Karpowicz et al., 2010; Li et al., 2014, 2015; Meng et al., 2015; Ren et al., 2010; Shaw et al., 2010; Staley and Irvine, 2010; Zheng et al., 2015).

The intestinal epithelium is an inside-out layer that has tight junctions to separate internal tissues from the outside environment (Clark and Walker, 2018; Garcia-Hernandez et al., 2017; Harden et al., 2016; Vancamelbeke and Vermeire, 2017). Insects have the equivalent septate junctions: in endoderm-derived tissues such as the midgut they are called smooth septate junctions, while in ectoderm-derived tissues such as imaginal discs they are called pleated septate junctions (Furuse and Izumi, 2017). Various upstream components, including junction proteins, have been implicated in regulating the Hpo pathway (Boggiano and Fehon, 2012; Li et al., 2018; Ma et al., 2018; Meng et al., 2018; Misra and Irvine, 2018; Poon et al., 2018; Yu and Pan, 2018). Meanwhile, conserved components of smooth septate junctions in silkworm and *Drosophila*, including two transmembrane proteins called Snakeskin (Ssk) and Mesh, have been implicated in adult midgut homeostasis (Izumi et al., 2012, 2019; Salazar et al., 2018; Yanagihashi et al., 2012). Here, we illustrate the genetic and molecular functions of Ssk and Mesh in EBs and ECs of adult *Drosophila* midgut, involving direct regulation of Yki to modulate the expression of Upd3 and thereby ISC division and intestinal homeostasis.

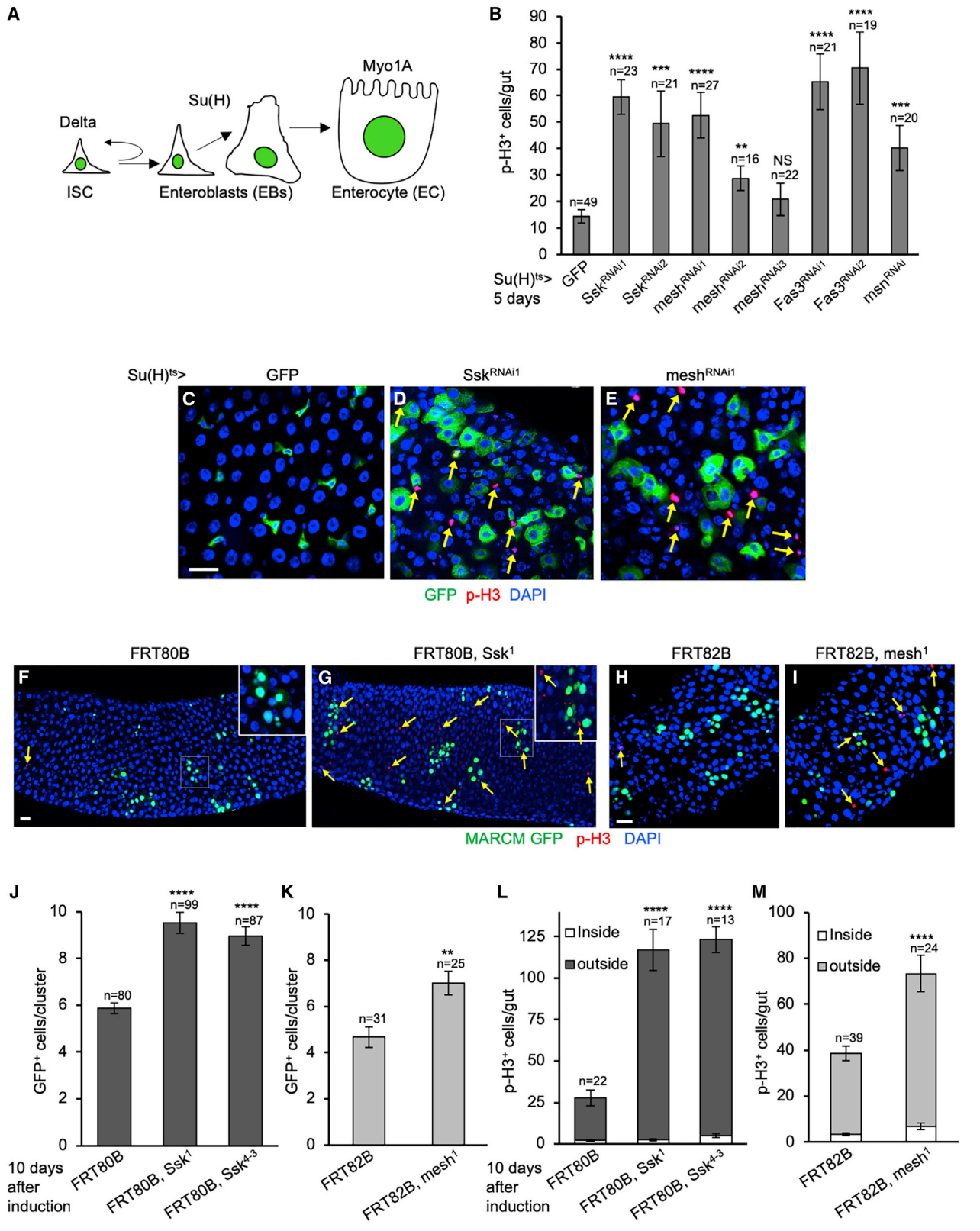

(legend on next page)

RESULTS

Loss of Smooth Septate Junction Proteins in EBs Leads to ISC Proliferation

We used the Su(H)Gbe promoter-Gal4, UAS-GFP; tubulin-Gal80^{ts} (abbreviated as Su(H)^{ts} > GFP) temperature-sensitive strain as the driver and marker for RNA interference (RNAi) of membrane-associated proteins in EBs, because EBs have been shown to produce factors that regulate ISC proliferation (Figure 1A) (Antonello et al., 2015; Cordero et al., 2012; Doupe et al., 2018; Li et al., 2014, 2018). The knockdown of *msn* and *Tao* produced highly increased numbers of GFP$^+$ cells and served as controls (citation here needs change) (Figure 1B and Table S1) (Li et al., 2014, 2018). Although knockdown of adherens junction, Hippo signaling, and other pathways occasionally gave mild increases in GFP$^+$ cells, knockdown of many septate junction components, including *Ssk*, *mesh*, and *Fasciclin3* (*Fas3*) led to a more noticeable increase (Table S1, and full list in https://figshare.com/s/c3a3931f9908880fe1cd). Quantification of mitotic ISCs by antibody staining for phosphorylated-histone3 (p-H3) (Amcheslavsky et al., 2009; Micchelli and Perrimon, 2006; Ohlstein and Spradling, 2006) showed that multiple *Ssk*, *mesh*, or *Fas3* RNAi lines all induced midgut proliferation and increased number of GFP$^+$ precursor cells (Figures 1B and 1C–1E).

We used the CRISPR/Cas9 gene engineering to generate insertion-deletions in *Ssk* or stop codons in *mesh* (Figures S1A and S1B). These CRISPR-generated *Ssk* and *mesh* mutants were homozygous lethal, similar to the other mutant combinations reported previously (Izumi et al., 2012; Yanagihashi et al., 2012). We used the mosaic analysis with repressible cell marker (MARCM) technique (Lee and Luo, 2001) to study their functions in adult midgut. The *Ssk* and *mesh* mutations were generated on FRT80B or FRT82B parental chromosomes, which allow the generation of homozygous mutant clones marked with GFP in otherwise heterozygous animals (Figures 1F–1I). Ten days after clone induction, both *Ssk* and *mesh* mutants had significant albeit modest increase in clone size when compared with those in parental strains, suggesting an increased ISC proliferation (Figures 1J and 1K). More importantly, we observed that the increase in p-H3$^+$ cells was more obvious when more mutant cells were present, and the majority of p-H3$^+$ cells were located outside the GFP$^+$ mutant clones (Figures 1L and 1M). These results suggest that *Ssk* and *mesh* loss-of-function mutant clones increase not only their own proliferation but also the proliferation of surrounding wild-type ISCs, and thus can act through an ISC-non-autonomous mechanism. The quantification of Delta$^+$ ISCs, Prospero$^+$ EEs, and p-H3$^+$ mitotic cells within the clones (Figure S2) revealed that there was no significant increase in these cell types. The number of

Figure 1. Loss of Smooth Septate Junction Proteins in EBs Leads to ISC Proliferation

(A) An illustration of ISC asymmetric division and enteroblast (EB)-enterocyte (EC) differentiation lineage in the adult *Drosophila* midgut. Delta is an ISC marker, Su(H) is expressed in EBs, and Myo1A is expressed in ECs.

(B) A graph showing the average number of p-H3$^+$ cells per whole midgut after crossing with the Su(H)^{ts}Gal4 driver, and temperature shifted to 29°C for 5 days to inactivate the Gal80^{ts} repressor to allow Gal4-dependent expression of UAS-dsRNA from the indicated transgenic lines. The control is UAS-GFP, which is also included in all the RNAi experiments.

(C) A confocal image showing surface view of a midgut from a control fly with the Su(H)^{ts}Gal4 driver and UAS-GFP transgenes.

(D) Image of a midgut from a similar cross with an additional UAS-*Ssk* RNAi transgene.

(E) Image of a midgut from a similar cross with an additional UAS-*mesh* RNAi transgene.

(F) Image of a MARCM experiment using control FRT80 flies, and the gut was also stained for p-H3, shown in red. The arrow indicates a p-H3$^+$ mitotic cell. A representative clone with GFP is shown in the enlarged image.

(G) Image of a similar MARCM experiment using the *Ssk^1* mutant flies. Arrows indicate p-H3$^+$ cells, some of them are inside the clones but many are outside the clones. The enlarged image shows an example of both.

(H) Image of a similar MARCM experiment using control FRT82B flies.

(I) Image of a similar MARCM experiment using the *mesh^1* mutant flies.

(J) Quantification of the parental *FRT80* alleles and the two different *Ssk* mutants used for MARCM, and individual clone size is the number of GFP$^+$ cells in a cluster. More than 30 clones were counted in each experiment and the average is plotted as shown.

(K) Similar MARCM experiments using the *mesh^1* mutant and the parental *FRT82*B alleles.

(L) Quantification of mitotic cells by p-H3 staining in MARCM gut. Those p-H3$^+$ cells that also had GFP were counted as inside the MARCM clones (white portion). Those p-H3$^+$ cells that had no GFP were counted as outside the MARCM clones (gray portion).

(M) Similar MARCM experiments using the *mesh^1* mutant and the parental *FRT82*B alleles to quantify p-H3$^+$ cells that are inside or outside the clones.

For all images in this figure, green is GFP, blue is DAPI for DNA, arrows indicate some of the p-H3 staining in red. Scale bars represent 20 μm. For all graphs, error bars are standard error of the means, and p values are represented as **p < 0.01, ***p < 0.001, ****p < 0.0001. NS is no significance. Statistics were based on unpaired Student's t test. The n value represents the number of guts or clones used for counting the indicated staining.

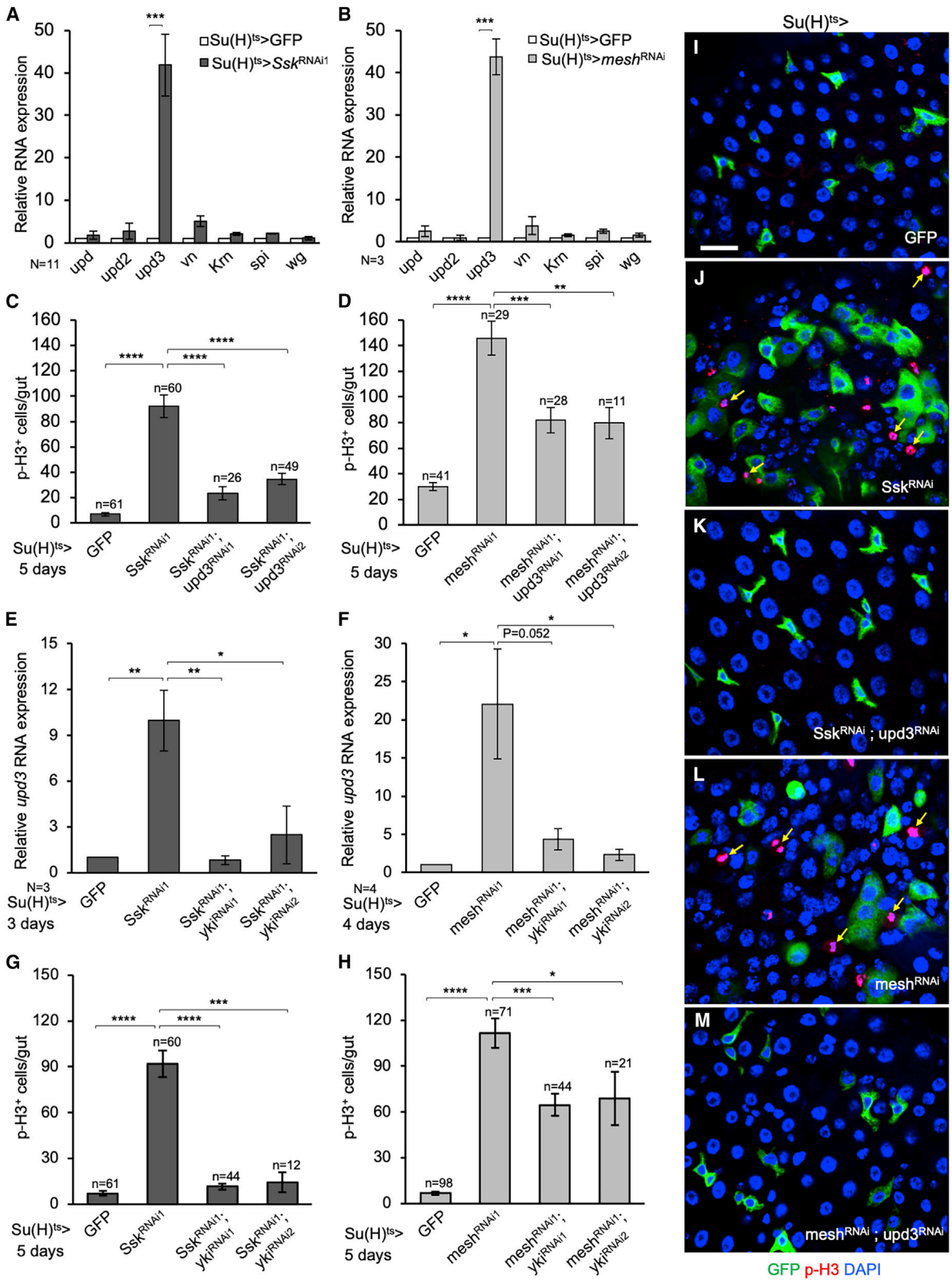

(legend on next page)

ECs in MARCM clones by Pdm1 antibody staining (Figures S2C and S2D) showed that ECs were increased in *Ssk* or *mesh* mutants, similar to the clone size increase. These results are consistent with the idea that there is increased proliferation and no obvious defect in differentiation along the EB-EC lineage in the mutants, therefore resulting in the midgut hyperplasia phenotype as observed.

Yorkie and Upd3 Mediate Growth after Loss of Ssk or Mesh

An ISC-non-autonomous mechanism would predict that loss of *Ssk* or *mesh* causes the secretion of a growth factor that can increase ISC proliferation. An assay for multiple ligands revealed that the expression of *upd3*, which encodes a ligand of the JAK-STAT pathway, was robustly increased in terms of fold change (Figures 2A and 2B). Double knockdown experiments using the Su(H)^{ts} > driver and two independent *upd3* RNAi constructs caused significant suppression of the mitotic cell numbers (Figures 2C and 2D). Confocal imaging (Figures 2I–2M) also revealed that, in the double RNAi samples, the Su(H)^{ts} > driven GFP^{+} cell number and organization resembled that of wild-type gut. It is noteworthy that the suppression of mitotic counts in the *mesh*;*upd3* double RNAi experiments were only approximately 50% (Figure 2D), suggesting that loss of *mesh* may activate additional factors, such as Vein, Keren, and Spitz, of the epidermal growth factor pathway (Figures 2A and 2B), to stimulate growth.

Previous reports demonstrate that the expression of *upd3* in the adult midgut can be regulated by multiple pathways, including the Wts-Yki pathway (Houtz et al., 2017; Li et al., 2014, 2018). The kinase Wts phosphorylates and inhibits Yki. When this phosphorylation is reduced, Yki is released and acts as a transcriptional coactivator. Therefore, we tested the requirement of Yki by using Su(H)^{ts} > to drive the expression of two different *yki* RNAi strains in EBs. The inclusion of *yki* RNAi highly reduced the expression of *upd3* RNA (Figures 2E and 2F), and the mitotic counts, very similar to that by *upd3* RNAi (compare Figures 2G and 2H with Figures 2C and 2D). Addition of a control UAS-mCherry RNAi did not provide such suppression (Figure S4D).

Ssk and Mesh Expression and Function Are Initiated in EBs to Produce Upd3 for ISC Proliferation

The strong midgut proliferation phenotypes induced by using the EB driver suggest that either Ssk and Mesh have a function within EBs or that the RNAi effects sustain long enough into ECs during maturation. We generated endogenously tagged knockin alleles that express Ssk-streptavidin-binding protein (Ssk^{ki-SBP}) and Mesh-V5 (Mesh^{ki-V5}) (Figure S1C) to investigate their expression in midgut cells. Although high levels of SBP and V5 staining were observed along cytoplasmic membranes of ECs, we also detected some cytoplasmic punctate staining in EBs (Figures 3A and 3B, arrows). Phalloidin stains for actin bundles in

Figure 2. Yorkie and Upd3 Mediate the Growth after Loss of Ssk or Mesh

(A) Quantification of RNA expression of the indicated genes by qPCR of total RNA isolated from guts of control (GFP) or *Ssk* RNAi flies driven by the Su(H)^{ts}-Gal4. Parallel PCR reactions using the *rp49* primers were used as the reference and the expression of each gene was normalized to that of *rp49* and set as 1 in control samples (white bars). The expression level of each gene in the *Ssk* RNAi fly guts was normalized to that of rp49 and then calculated as fold change compared with that in control.

(B) Similar qPCR quantification of the genes and showing the relative expression in *mesh* RNAi flies compared with the control.

(C) The graph shows the average mitotic counts in midguts of flies with the indicated control GFP, and *Ssk* plus *upd3* RNAi lines, driven by the Su(H)^{ts}-Gal4.

(D) Similar experiment showing the mitotic counts of control, and *mesh* plus *upd3* RNAi lines.

(E) Quantification of *upd3* RNA expression in adult midguts of the indicated control, *Ssk*, and *yki* RNAi lines. Each qPCR was compared with that of *rp49* as internal control and set as 1 in the control GFP sample. Other samples were plotted as fold change compared with the control. The 29°C incubation was for 3 days.

(F) Quantification of *upd3* RNA expression in adult midguts of the indicated control, *mesh*, and *yki* RNAi lines. The 29°C incubation was for 4 days.

(G) Mitotic counts in adult midguts of the indicated control, *Ssk* and *yki* RNAi lines after 5 days of incubation at 29°C driven by the Su(H)^{ts}Gal4. The dissected guts were staining for p-H3 and counted throughout the whole midgut. The average number is plotted.

(H) Mitotic counts in adult midguts of the indicated control, *mesh*, and *yki* RNAi lines.

(I) A representative confocal image showing surface view of a midgut from control flies of the genotype Su(H)^{ts} > GFP.

(J) A confocal image showing surface view of a midgut from Su(H)^{ts} > GFP,*Ssk*^{RNAi} flies. The arrows indicate some of the nuclear p-H3^{+} cells in red. More GFP^{+} cells also illustrate increased proliferation in the midgut.

(K) A confocal image showing surface view of a midgut from Su(H)^{ts} > *Ssk*^{RNAi},*upd3*^{RNAi} flies.

(L) A confocal image showing surface view of a midgut from Su(H)^{ts} > *mesh*^{RNAi} flies.

(M) A confocal image showing surface view of a midgut from Su(H)^{ts} > *mesh*^{RNAi},*upd3*^{RNAi} flies.

Statistics were based on unpaired Student's t test. The n value represents the number of guts used for counting the indicated staining. The N value represents the number of biological repeats of the experiments.

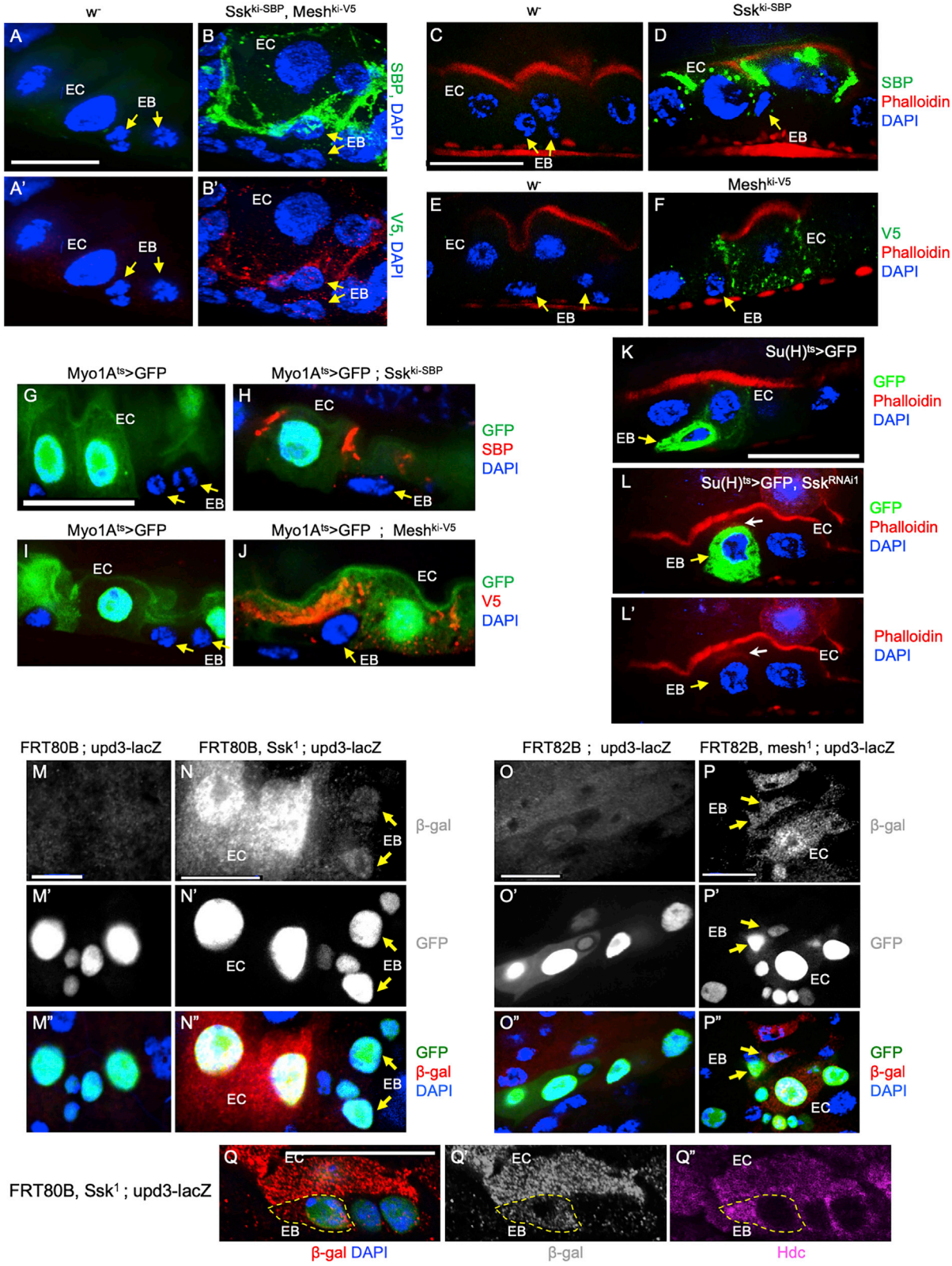

(legend on next page)

apical brush borders of mature ECs (Figures 3C–3F) and Myo1A > GFP (Figures 3G–3J) label mature ECs; the staining of these two EC markers was distinct from the smaller EBs that had low but detectable cytoplasmic SBP and V5 (Figures 3C–3J, arrows). Furthermore, the precursor cell nests have high-level expression of armadillo/β-catenin. Double staining of armadillo with the knockin Mesh-V5 illustrated detectable expression of Mesh in EBs (Figures S3A and S3B). In addition, direct labeling of EBs by the Su(H)-promoter-LacZ reporter illustrated the presence of SBP staining in these EBs (Figures S3F and S3G).

Multiple lines of experiments demonstrated that Su(H)^{ts} > driven *Ssk* or *mesh* RNAi caused an increased proliferation and continuous differentiation of EBs to ECs. First, among the GFP$^+$ progenies, some were of medium size, not yet fully integrated with ECs, but had low levels of phalloidin staining (Figure 3L, arrow). Second, most of those Su(H) > GFP marked cells of varying sizes still expressed the EB marker Headcase (Hdc) (Figures S3C–S3E) (Resende et al., 2017). This is consistent with the increased expression of Upd3, which can activate the JAK-STAT pathway to promote ISC proliferation and subsequent differentiation, as reported previously (Jiang et al., 2009; Xu et al., 2011; Zhou et al., 2013). In contrast, the *Ssk* or *mesh* RNAi within ISCs by the Delta-Gal4 driver even for prolonged periods did not show an increased proliferation phenotype (Figure S3H).

To ascertain that the JAK-STAT pathway ligand Upd3 is produced within EBs, we crossed a 4-kb *upd3* promoter-driven lacZ reporter to the *Ssk* or *mesh* mutants and performed MARCM (Li et al., 2014; Zhou et al., 2013). The MARCM results showed that 76.6% of the *Ssk* mutant GFP$^+$ clones (n = 141) versus 21.2% of the FRT80 control clones (n = 146) also contained β-galactosidase staining (Figure S2J). Similarly, 83.5% of *mesh* mutant clones (n = 94) versus 21.1% of the FRT82B control clones (n = 57) had β-galactosidase and GFP co-staining (Figure S2K). These results demonstrate that the *upd3* reporter is expressed largely within the mutant cells. Confocal imaging revealed that the β-galactosidase staining in *Ssk* or *mesh* mutant clones was not obvious in ISCs and early EBs (small cells), but became detectable in EBs of medium size (arrows

Figure 3. Ssk and Mesh Expression and Function Are Initiated in EBs to Produce Upd3 for ISC Proliferation

(A) Control staining for SBP and V5 around a cell nest using the parental w^- fly gut. The arrows indicate EBs based on the size.

(B) Confocal images of staining for SBP and V5 using guts from flies with both the knockin alleles crossed together. High level staining appears in circumference of the EC, and low level punctate staining is also present in EBs, indicated by arrows. The images in (A and B) are single optical sections of 0.2 μm each.

(C) Confocal image of longitudinal cross-section of w^- control midgut, showing double Phalloidin staining in red for F-actin and SBP staining in green. The brush border of ECs at the apical side and the smooth muscle at the basal side had high levels of Phalloidin staining. The EBs are indicated by arrows and did not show red or green staining.

(D) Similar double staining using the Ssk^{ki-SBP} flies. The EB indicated by an arrow showed cytoplasmic punctate SBP staining, but not Phalloidin staining. The more apically located large ECs were labeled strongly with Phalloidin as well as strong SBP staining at junctions and cytoplasmic puncta.

(E) Similar w^- control midgut double stained with Phalloidin in red and V5 in green.

(F) Similar Mesh^{ki-V5} midgut double stained with Phalloidin in red and V5 in green. The smaller EB indicated by an arrow also showed cytoplasmic punctate V5 staining.

(G) Confocal image of control Myo1A^{ts} > GFP midgut, with GFP expressed only in ECs. Co-staining with SBP did not show any signal in EBs, indicated by arrows.

(H) Similar staining shows SBP cytoplasmic puncta in an EB that had no GFP, indicated by an arrow.

(I) Similar V5 staining showing no signal in EBs indicated by arrows of control Myo1A^{ts} > GFP midgut.

(J) Similar V5 staining showing cytoplasmic puncta in an EB, which is not labeled with GFP.

(K) Confocal image of a gut from control Su(H)^{ts} > GFP strain. The arrow indicates an EB that had strong GFP expression and no Phalloidin.

(L and L′) Confocal image of a gut from Ssk RNAi flies. The arrow indicates an EB of medium size that had both a GFP signal and weak apical Phalloidin staining (white arrow), suggesting that it was an EB continuing with its differentiating.

(M, M′, M″) A high magnification confocal image showing a GFP$^+$ MARCM clone from FRT80B control flies that also contained the *upd3*-promoter-*LacZ* reporter. The staining is shown in white in (M) and (M′). The staining is shown as green for GFP and red for β-galactosidase in (M″).

(N) A similar confocal image showing a GFP$^+$ MARCM clone from *Ssk^1* mutant flies. The arrows indicate EBs with detectable levels of β-galactosidase protein staining, expressing *upd3*. Note that ECs had higher levels of β-galactosidase.

(O) A confocal image showing a GFP$^+$ MARCM clone from FRT82B control flies that also contained the *upd3*-promoter-*LacZ* reporter.

(P) A similar confocal image showing a GFP$^+$ MARCM clone from *mesh^1* mutant flies. The arrows indicate EBs with detectable levels of β-galactosidase, expressing *upd3*.

(Q, Q′, Q″) Confocal images of a MARCM mutant clone form *Ssk^1* mutant flies that also contained the *upd3*-promoter-*LacZ* reporter. The gut was double stained for Hdc, which is expressed in EB cytoplasm. The dotted lines delineate the *Ssk* mutant EB with detectable levels of β-galactosidase and also Hdc staining, indicating that it was a differentiating EB expressing *upd3*.

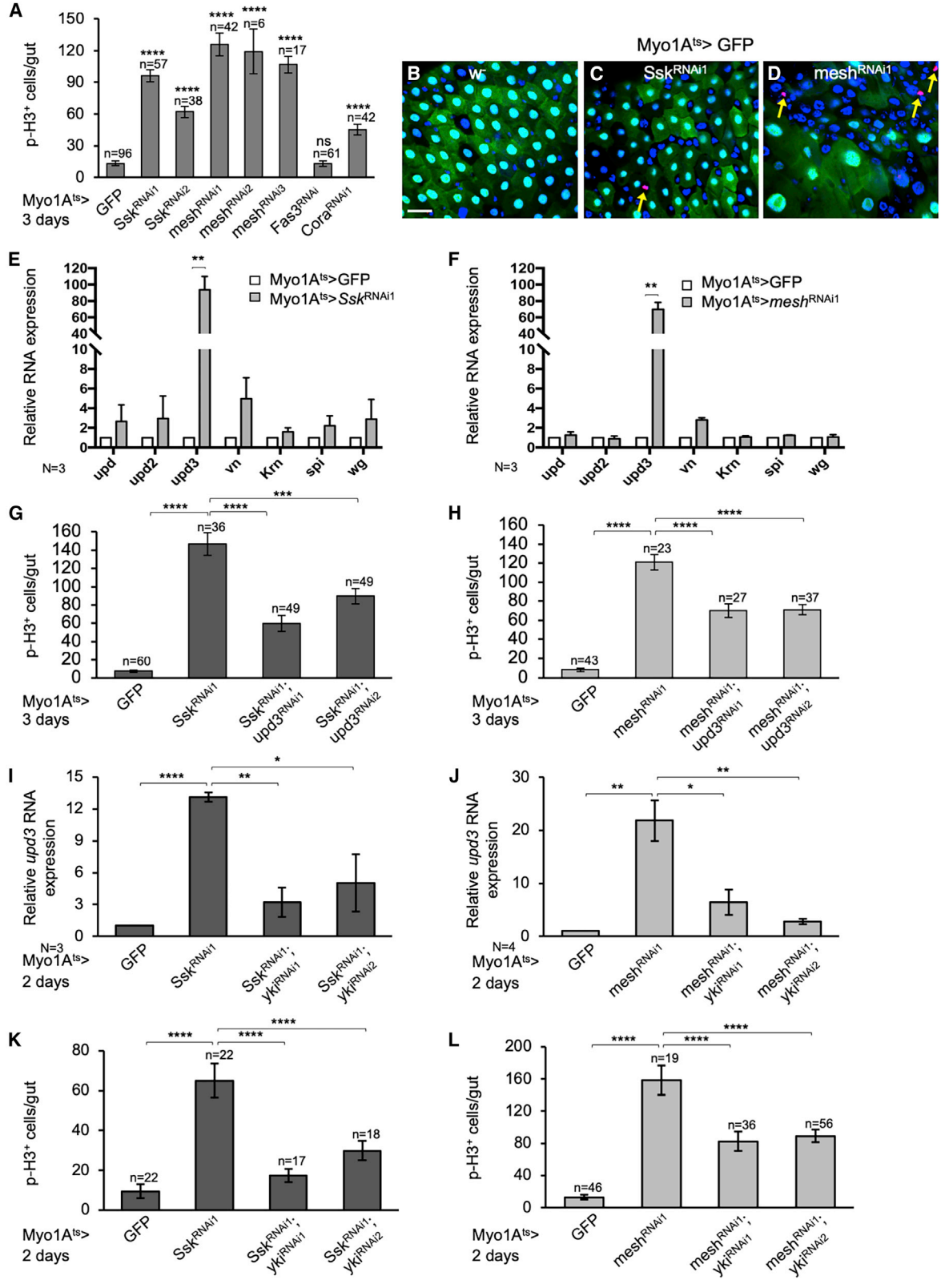

(legend on next page)

in Figures 3N and 3P). Further staining showed that these medium-sized upd3-LacZ-expressing cells also expressed the EB marker Hdc (Figure 3Q). Altogether, we conclude that loss of Ssk or Mesh function is sufficient to initiate the expression of Upd3 within EBs.

Ssk and Mesh Also Have Functions in ECs to Regulate Yorkie-Upd3 and Thereby ISC Proliferation

Because septate junctions in the gut are mainly associated with mature ECs, we examined whether *Ssk* and *mesh* are similarly required in ECs to regulate ISC proliferation, by using the Myo1A-Gal4, UAS-GFP; tubulin-Gal80^{ts} (Myo1A^{ts}>) driver. Multiple RNAi lines of *Ssk* and *mesh* caused highly increased mitotic counts (Figure 4A). In comparison, a *Coracle* (*Cora*) RNAi line only caused a moderate increase in proliferation, while a *Fas3* RNAi line did not result in an increase. There were also fewer GFP^{-} cells around the Myo1A^{ts} > GFP labeled big ECs (Figures 4B–4D), illustrating that there was accumulation of precursor cells as a result of increased ISC division. We have examined many samples and images, and overall there is no individual cell growth increase of phenotypes, but instead faster differentiation along the EB-EC lineage, becoming polyploid and therefore bigger. This is consistent with increased expression of the growth factor Upd3.

The knockdown of *Ssk* or *mesh* by RNAi in ECs also resulted in highly increased expression of *upd3* (Figures 4E and 4F). The Myo1A^{ts} > driven *upd3* RNAi suppressed significantly, although not completely (40%–50%), the ISC proliferation induced by *Ssk* or *mesh* RNAi (Figures 4G and 4H). Meanwhile, we performed time course *yki* RNAi experiments and the results suggest different requirements of Yki at different times in ECs. Although 1 day of *Ssk*/*mesh* RNAi was not sufficient to induce a significant increase in proliferation (Figure S4C), 2 days of RNAi caused an increase in both *upd3* expression and mitotic counts. Importantly, the inclusion of *yki* RNAi after 2 days of induction caused significant suppression of these phenotypes (Figures 4G–4J). The addition of a control UAS-mCherry RNAi again did not provide such suppression (Figure S4E). If the temperature shift to induce RNAi was carried out for 3 days, the mitotic counts, however, remained high in the double RNAi samples (Figures S4A and S4B). It is possible that prolonged knockdown of *Ssk* or *mesh* in ECs may cause a substantial loss of septate junctions, followed by lethality (see Figure 6), and therefore might mobilize additional stress-response pathways. However, we did not detect an involvement of the JNK pathway (Figures S5A–S5D) or substantial cell death (Figures S5E–S5H) after 2–3 days of knockdown of *Ssk* or *mesh* in ECs, suggesting an involvement of other pathways.

The Ssk-Mesh Complexes Are Required for Co-localization with Other Junction Proteins in ECs

We used the knockin alleles of Ssk and Mesh to perform a series of experiments to investigate whether these two components are critical for septate junction formation in ECs. Both endogenous fusion proteins Ssk^{ki-SBP} and Mesh^{ki-V5} formed a ring around the membrane of ECs, as well as some cytoplasmic punctate staining especially for Mesh (Figure 5A). Longitudinal cross-section view of this staining revealed that the two proteins were co-localized to apical-lateral positions, as expected for septate junctions (Figure 5B, arrowheads), and the two proteins can be co-immunoprecipitated from adult gut extracts (Figure 5C). Moreover, the localization of Ssk and Mesh at the junctions are dependent on each other, because RNAi caused dispersion of immunofluorescent signals from the junctions (Figures 5D–5G).

Figure 4. Ssk and Mesh Also Have Functions in ECs to Regulate Yorkie-Upd3 and Thereby ISC Proliferation

(A) The graph shows the average number of p-H3^{+} cells per whole midgut from adult flies after crossing with the various indicated RNAi lines with the Myo1A^{ts} > driver, and the temperature shift was for 3 days.

(B) Confocal image of a midgut from a control flies crossed with the Myo1A^{ts} > UAS-GFP. All ECs cells are GFP^{+}, and other cells are GFP^{-}.

(C) Confocal image of a midgut from a similar cross with an additional UAS-*Ssk* RNAi transgene. The arrow indicates a p-H3^{+} staining.

(D) Confocal image of a midgut from a similar cross with an additional UAS-*mesh* RNAi transgene. The arrows indicate p-H3^{+} staining.

(E) Quantification of RNA expression by qPCR of the indicated genes from gut samples with the Myo1A^{ts} > driver crossed with control or *Ssk*^{RNAi}. The temperature shift was for 3 days.

(F) Similar quantification of RNA expression as in (E), except using the *mesh*^{RNAi}.

(G) Quantification of p-H3^{+} cells from whole guts of flies after crossing the Myo1A^{ts}> with the indicated single or double *Ssk* and *upd3* RNAi lines. The temperature shift was for 3 days.

(H) Similar quantification of p-H3^{+} cells, except using the *mesh*^{RNAi}.

(I) Quantification of *upd3* RNA expression by qPCR. Whole guts were obtained from flies after crossing the Myo1A^{ts}> with the indicated RNAi lines. Note that the temperature shift was shorter, for 2 days.

(J) Similar quantification of *upd3* RNA expression, except using the *mesh*^{RNAi}.

(K) Quantification of p-H3^{+} cells from whole guts of flies after crossing the Myo1A^{ts}> with the indicated RNAi lines. Note that the temperature shift was for 2 days. (L) Similar quantification of p-H3+ cells, except using the *mesh*^{RNAi}.

Statistics were based on unpaired Student's t test. The n value represents the number of guts used for counting the indicated staining. The N value represents the number of biological repeats of the experiments.

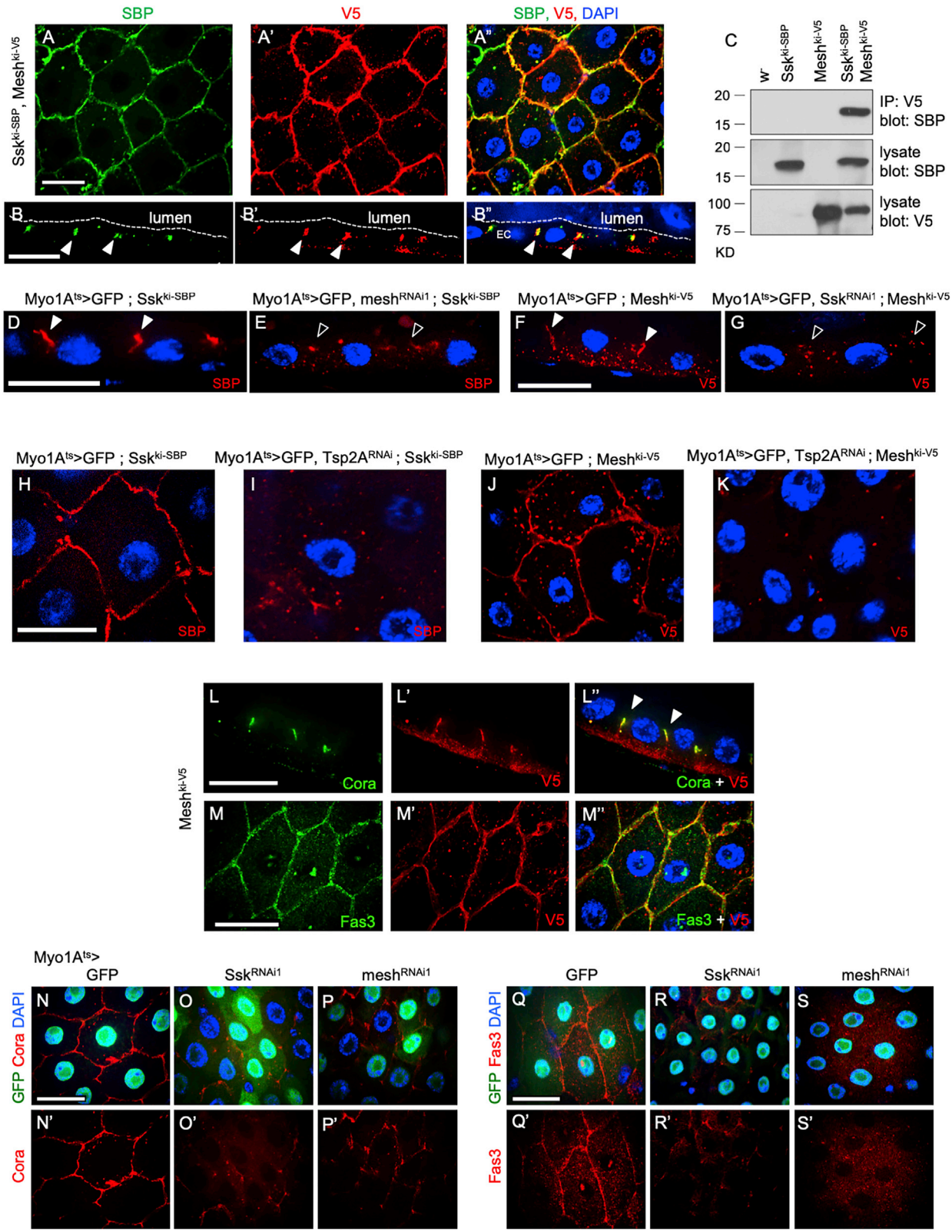

(legend on next page)

Previous reports illustrate that Ssk, Mesh, and Tsp2A are likely components of smooth septate junctions in developing *Drosophila* embryos and larvae (Izumi et al., 2012, 2016; Yanagihashi et al., 2012). Recent reports also implicate these three proteins in adult midgut homeostasis (Izumi et al., 2019; Salazar et al., 2018; Xu et al., 2019). Our results also showed that the junction localization of Ssk and Mesh were dependent on Tsp2A (Figures 5H–5K). Cora and Fas3 are known to associate with septate junctions in other epithelial tissues (Boggiano and Fehon, 2012) and are involved in adult midgut proliferation to varying degrees (see Figures 1B, 1C, and 4A). The staining of Cora and Fas3 matched that of Mesh at the junctions of ECs (Figures 5L and 5M), and their localization was largely disrupted after *Ssk* or *mesh* RNAi (Figures 5N–5S).

Loss of Ssk and Mesh in EBs or ECs Leads to Different Degrees of Gut Leakiness and Animal Viability

Septate junctions provide the barrier function essential for epithelial integrity and animal viability (Furuse and Izumi, 2017; Garcia-Hernandez et al., 2017; Harden et al., 2016; Rera et al., 2012; Resnik-Docampo et al., 2018; Vancamelbeke and Vermeire, 2017). Because Ssk and Mesh have functions in both EBs and ECs, we examined how these two cell types contribute to gut barrier function and whole animal viability. Leaky gut can lead to the accumulation of a blue dye in the body cavity after the dye is fed to flies, termed as Smurf assay (Rera et al., 2012). We found that 3 days of *Ssk* or *mesh* RNAi in EBs led to less than 3% of the flies exhibiting the Smurf phenotype (Figure 6A). The number of dead flies was also limited and closely correlated with the Smurf phenotype (Figure 6B). Meanwhile, the same experiment using the EC driver resulted in approximately 10% of flies having the Smurf phenotype after 3 days, and that subsequently increased sharply (Figure 6C). The lethality was closely correlated with the profile of the Smurf assay (Figure 6D). Therefore, Ssk and Mesh have an essential barrier function in ECs, where the disruption of this complex leads to loss of tissue integrity, followed by lethality, as shown recently for Ssk (Salazar et al., 2018). Meanwhile, the loss of Ssk and Mesh in EBs has only minor effects on leakiness and viability. Considering the strong ISC proliferation phenotype after loss of Ssk and Mesh in EBs, we speculate that the cytoplasmic localization of Ssk and Mesh in EBs is sufficient to regulate downstream signaling components for intestinal homeostasis.

Figure 5. The Ssk-Mesh Complex Are Required for the Co-localization with Other Junction Proteins in ECs

(A, A′, and A″) Confocal images of surface view of an adult midgut from flies harboring both Ssk^{ki-SBP} and $Mesh^{ki-V5}$. Co-immunostaining was using antibodies for SBP shown in green in (A), and for V5 shown in red in (A′). The double color together with DAPI is shown in (A″). The focal plan of the images was around the apical side of ECs, where the smooth septate junctions are expected to locate. Some punctae are also observed in the cytosol of ECs.

(B, B′, and B″) Confocal images of longitudinal cross-section view of a midgut from flies harboring Ssk^{ki-SBP} and $Mesh^{ki-V5}$. The SBP and V5 staining co-localized at presumed septate junctions indicated by the arrowheads near the apical side of ECs. The white dash line indicates the apical border of the epithelium adjacent to the gut lumen.

(C) Western blots showing co-immunoprecipitation of the Ssk^{ki-SBP} and $Mesh^{ki-V5}$ proteins, using extracts prepared from the w^- control, single knockin, and double knockin fly guts. The extracts were used for V5 immunoprecipitation and then SBP western blots, or for western blots directly in the two lower panels as indicated.

(D) Confocal image of longitudinal cross-section view of SBP staining of gut from control flies crossing the Ssk^{ki-SBP} with the $Myo1A^{ts}$ > GFP. The staining is tightly localized to the EC junctions indicated by arrowheads.

(E) Similar SBP staining except the flies also included the $mesh^{RNAi}$ construct, which caused disruption of staining at the junctions (open arrowheads).

(F) Similar V5 staining in control guts.

(G) Similar V5 staining in guts that also included Ssk^{RNAi}.

(H) Confocal image of surface view of SBP staining in control gut.

(I) Similar SBP staining except the flies also included the $Tsp2A^{RNAi}$ construct.

(J) Similar V5 staining in control guts.

(K) Similar V5 staining except the flies also included the $Tsp2A^{RNAi}$ construct.

(L, L′, and L″) Confocal image of longitudinal cross-section view of gut from the $Mesh^{ki-V5}$ fly strain stained for V5 and Cora. The arrowheads in (L″) indicate co-localization at the apical junctions of the two proteins.

(M, M′, and M″) Confocal image of surface view of similar gut stained for V5 and Fas3. The confocal section is 0.2 μm and the two proteins had almost identical pattern around the cell membrane.

(N and N′) Confocal image of surface view of control gut expressing $Myo1A^{ts}$ > GFP and stained for Cora.

(O and O′) Similar image showing Cora from membrane junction was dispersed after Ssk^{RNAi}.

(P and P′) Similar image showing Cora staining was dispersed after $mesh^{RNAi}$.

(Q and Q′) Confocal image of control gut expressing $Myo1A^{ts}$ > GFP and stained for Fas3.

(R and R′) Similar image showing Fas3 from membrane junction was dispersed after Ssk^{RNAi}.

(S and S′) Similar image showing Fas3 staining was dispersed after $mesh^{RNAi}$.

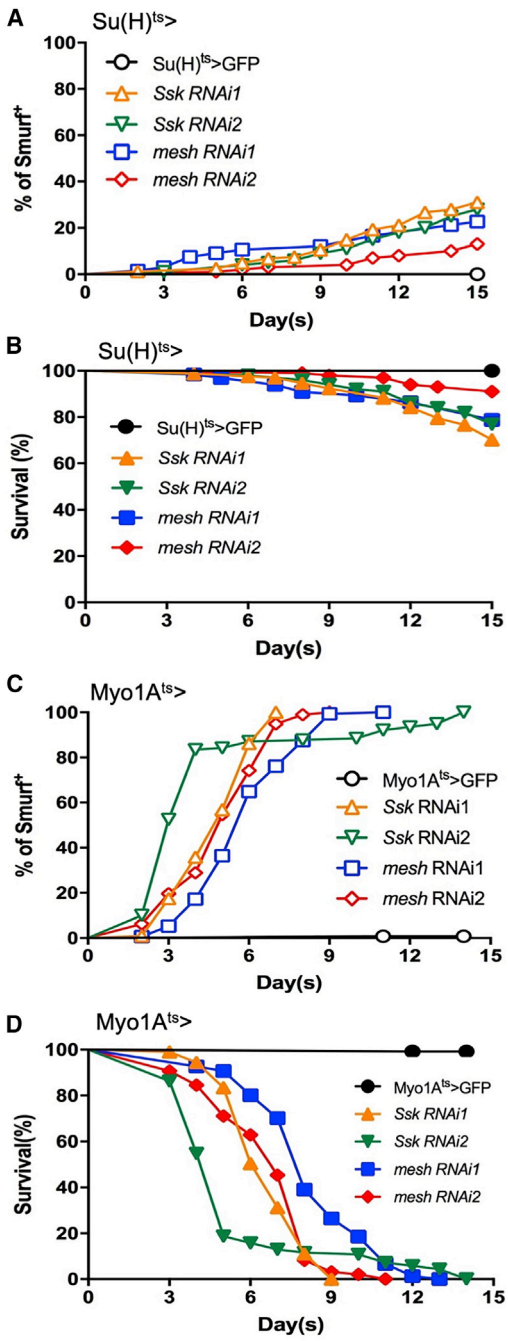

Figure 6. Loss of Ssk and Mesh in EBs and ECs Leads to Different Degrees of Gut Leakiness and Animal Viability

(A) Quantification of Smurf flies after feeding with food dye to flies with the indicated genotypes. Standard fly medium was mixed with blue dye. Newly eclosed flies were aged for 3 days on standard medium under room temperature and 50 flies were placed on dyed medium at 29°C. The flies were counted every day. The cumulative percent of Smurf^{+} flies after each day is plotted as shown.

(B) Quantification of viable flies with the indicated genotypes. Fifty flies were placed in regulated food vials. The food vials were changed and surviving flies counted every day. The cumulative percent of flies still alive after each day is plotted as shown.

(C) Similar quantification of Smurf flies, using the Myo1A^{ts}-Gal4 driver.

(D) Similar quantification of viable flies, using the Myo1A^{ts}-Gal4 driver.

The plots each is an average of three independent experiments for the indicated genotype.

Ssk and Mesh Form a Complex with and Restrict the Activity of Yki

In both EBs and ECs, the function of Yki is required to mediate the expression of Upd3, which in turn promotes ISC proliferation. At least two upstream Sterile20 kinases, Msn and Hpo, can phosphorylate and activate Wts, which in turn phosphorylate and inhibit Yki (Li et al., 2014, 2018; Ma et al., 2018; Misra and Irvine, 2018). On Phos-tag gels, highly phosphorylated Yki exhibited slower mobility and accumulated at the top of the gel. The faster-moving Yki proteins have lower phosphorylation (Figures 7A and 7B, arrows). *Ssk* or *mesh* RNAi caused reduced Yki phosphorylation, albeit at lower levels compared with that caused by *wts* RNAi (Figures 7A and 7B). One explanation is that Wts is a central kinase that receives many different upstream signals to regulate Yki, while the Ssk-Mesh complex may only represent one of the many upstream events and therefore only partially reduces Yki phosphorylation.

In the adult midgut, Msn is expressed and functions in EBs, while Hpo functions in ECs, to regulate Yki and subsequently ISC proliferation (Li et al., 2014, 2018). One mechanism that regulates Hpo and Msn activities is through phosphorylation of a conserved T187/T194 residue in their kinase domains (Li et al., 2018). We examined the phosphorylation of this activation site on transgenic constructs of Msn and Hpo after *Ssk* or *mesh* RNAi. However, we did not observe any consistent change of this phosphorylation (Figures S6A and S6B). Therefore, we speculated that Ssk and Mesh might interact with a downstream component. Co-immunoprecipitation experiments performed in transfected S2 cells showed that Yki could form a complex with Ssk, and in an independent experiment also with Mesh (Figures 7C and 7D). Co-transfection of Ssk and Mesh together with Yki in S2 cells but did not further increase the co-immunoprecipitation signal. The cultured S2 cells probably do not form septate junctions, but the transfection results nonetheless demonstrate that Ssk or Mesh when overexpressed in cells can bind directly or indirectly to Yki.

DISCUSSION

We have used knockin and knockout alleles of Ssk and Mesh to demonstrate their functions in both EBs and ECs

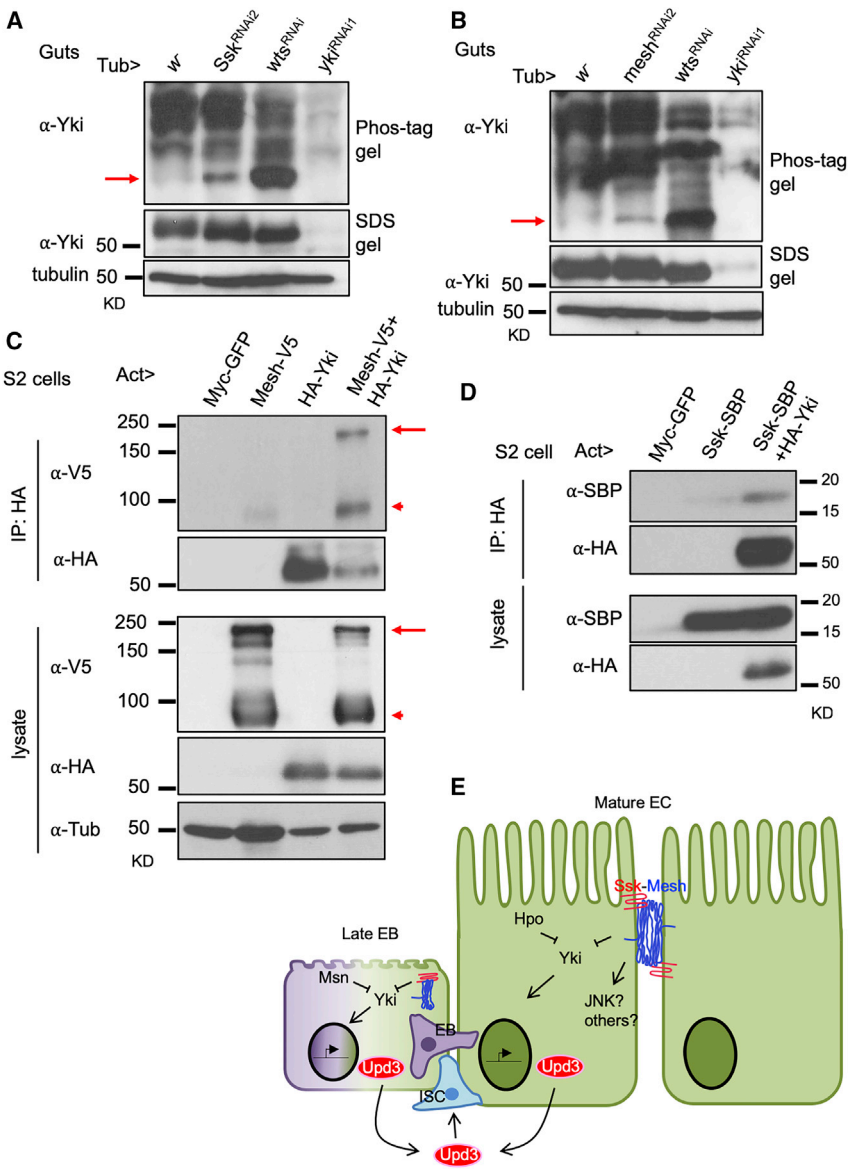

Figure 7. Ssk and Mesh Form a Complex with and Restrict the Activity of Yki

(A) Western blots using an antibody for endogenous Yki. Guts were dissected from flies with the tubulinGal4 ubiquitous driver and the indicated RNAi lines. Extracts were prepared and resolved on a Phos-tag gel for the upper panel, or regular SDS gel for the middle and lower panels. A Yki antibody was used for the upper and middle blots, and a tubulin antibody was used for the lower blot. The red arrow in the upper panel indicates the Yki protein that had the highest mobility, representing the lowest phosphorylation.

(B) A similar Phos-tag gel for Yki, except that *mesh* RNAi flies were used.

(C) Co-immunoprecipitation of Mesh and Yki in transfected S2 cells using the tagged protein expression constructs as indicated. The UAS expression constructs were co-transfected with ActinGal4 as the driver. The resulting extracts were used for immunoprecipitation by HA antibody, and blotted for V5 or HA. The lysates were also used for blots as expression control in lower panels. The red arrows indicate the expected size of full-length Mesh protein. The red arrowheads indicate the expected size of a truncate Mesh due to a protease cleavage site, as described previously (Izumi et al., 2012).

(D) A similar co-immunoprecipitation of Ssk and Yki in transfected S2 cells.

(E) A model illustrating the function of smooth septate junction proteins, Ssk and Mesh, in adult *Drosophila* midgut EBs and ECs. The expression of Ssk and Mesh are initiated in differentiating EBs and gradually incorporated into the smooth septate junction at the apical-lateral side of mature ECs. In addition to their barrier function, Ssk and Mesh also form a complex with Yki, in the cytoplasm, or at the membrane. This may spatially facilitate Yki phosphorylation and inhibition by upstream kinases Wts, Msn, or Hpo, or may restrict the mobilization of Yki, thereby providing a negative regulation of Yki. Change of septate junction-Yki interaction by mechanical stretching or by tissue damage may allow Yki to become more active to increase Upd3 expression and cause a change of midgut homeostasis.

to regulate ISC proliferation (Figure 7E). Ssk and Mesh have low but detectable expression in the cytoplasm of EBs, while that in ECs is mainly in septate junctions but also with some cytoplasmic localization. Multiple lines of evidence suggest that the Ssk and Mesh expression in EBs is of functional importance. First, the EB driver Su(H) > has expression in fewer cells when compared with the Myo1A > driver but still can cause comparable Upd3 expression and proliferation phenotypes. Second, mutant *Ssk* and *mesh* MARCM clones have detectable *upd3-promoter-LacZ* reporter expression in late EBs, and in addition to that in mature ECs. Third, the Su(H) > *Ssk* or *mesh* RNAi had very minor Smurf and lethality phenotype, suggesting that the EB RNAi effects do not linger into mature ECs, but yet can cause strong proliferation phenotypes.

Recent reports have expanded the Hpo/Mst pathway to include Msn and Hppy, as well as their mammalian homologs MAP4K1-7 (Li et al., 2014, 2015; Meng et al., 2015; Poon et al., 2018; Zheng et al., 2015). Many membrane-associated proteins, such as cadherin-like protein FAT, adherens junction protein α-catenin, and tight junction protein Angiomotin are involved in the Hpo/Mst pathway

by regulating upstream components (Dai et al., 2013; Fletcher et al., 2018; Han et al., 2018; Mana-Capelli et al., 2014; Mana-Capelli and McCollum, 2018; Meng et al., 2018; Su et al., 2017; Yu and Pan, 2018; Zhao et al., 2011). Our results here suggest that smooth septate junctions may act as a signaling platform by directly binding to Yki. That previous protein interaction screens conducted in S2 cells had not identified the Yki complex with Ssk or Mesh (Kwon et al., 2013; Yu and Pan, 2018) may be because Ssk and Mesh are expressed much more highly in the gut than in other tissues.

Another smooth septate junction component Tsp2A regulates midgut homeostasis through the aPKC-Hpo pathway, possibly involving endosomal trafficking (Xu et al., 2019). We also observed that Ssk and Mesh had detectable expression in cytoplasmic punctae (see Figures 3 and 5). However, Tsp2A can act in the whole ISC-EB-EC lineage (Xu et al., 2019), while we did not observe a function of Ssk and Mesh in early EBs. Therefore, it is possible that Mesh, Ssk, and Tsp2A can form a complex and are components of the smooth septate junction but each may also have independent functions.

Disruption of paracellular junctions in adult midgut leads to epithelial disorganization along the digestive track (Resnik-Docampo et al., 2018). Loss of tricellular junction protein Gliotactin leads to activation of the JNK pathway in ECs to stimulate ISC proliferation (Resnik-Docampo et al., 2017). Prolonged RNAi of *Ssk* and *mesh*, especially in ECs, leads to leaky gut and lethality, consistent with loss of septate junction integrity. The depletion of Yki alone after longer RNAi of *Ssk* or *mesh* in ECs, however, is not sufficient to suppress all the phenotypes, suggesting that such stress may stimulate multiple downstream response pathways. Regarding Yki target genes, *upd3* is the best-characterized target in the midgut. The other well-known targets from imaginal discs, including *DIAP1* and *Bantam*, are not good targets for Yki in the adult midgut. Meanwhile, one report (Kwon et al., 2015) shows that *ImpL2* expression is highly increased in response to over-activated Yki in the midgut, and regulates tissue metabolism. The physiological stimulation of *ImpL2* by Yki is still unclear. We have also assayed for *ImpL2* in the midgut after *Ssk* or *mesh* RNAi, but did not observe an increased expression of *ImpL2* (Figures S6C and S6D). We speculate that *ImpL2* may be a direct or indirect target related to metabolic phenotype induced by cancer-promoting genes, and therefore may not be regulated by the septate junction proteins Ssk or Mesh. Gut leakage may drive inflammation and trigger systematic immune response contributed by hemocytes, which in turn trigger ISC division indirectly (Chakrabarti et al., 2016). Further investigation will provide a more complete picture of how different pathways are involved.

EXPERIMENTAL PROCEDURES

Drosophila Stocks and Genetics

Strains used in this report and detailed experimental conditions are listed in Supplemental Information. For RNAi experiments, the final cross and progeny were maintained at room temperature and shifted to 29°C for 2–5 days for Myo1AGal4 and Su(H)Gal4 as specified in the figures. All Gal4-driven UAS-RNAi experiments also included the UAS-GFP as control and as marker for the cells that received the transgenes. The *Ssk* and *mesh* mutant and knockin tag alleles were generated by CRISPR/Cas9-mediated genome editing by non-homologous end-joining, or by homology-dependent repair. The mutant and knockin tag designs and injections were conducted by WellGenetics (Taipei, Taiwan). Mutant clones in adult midgut were generated by mitotic recombination using MARCM (Lee and Luo, 2001). Smurf assay was carried out using standard fly medium mixed with blue dye (FD&C Blue No. 1, SPS Alfachem) at a concentration of 2.5% (wt/vol) (Salazar et al., 2018).

Gut Dissection for Staining, RNA Isolation, and Protein Isolation

Female flies were used for gut dissection due to the bigger size. Adult flies aged for 5–7 days were used for RNAi induction or other manipulation before gut dissection. The entire gastrointestinal tracks were pulled out and fixed with 1× PBS plus 4% formaldehyde for staining, or in PBS without fixation for RNA and protein isolation. The buffers, antibodies, and reagents used, and immunostaining and fluorescent microscopy, are as published previously (Amcheslavsky et al., 2009; Li et al., 2014, 2018) and listed in Supplemental Information. For SYTOX cell death staining (Akagi et al., 2018), dissected guts were incubated with SYTOX Orange nucleic acid stain (Invitrogen, 1 μM) and Hoechst 33,342 (Invitrogen, 10 μg/mL) in pre-cold 1× PBS for 10 min at room temperature. Samples were quickly rinsed with 1× PBS twice, then mounted with 1× PBS and immediately analyzed using a Nikon Spinning Disk confocal microscope.

Molecular and Cellular Biology Assays

Transfection of S2 cells, Phos-tag gels, and western blot assays were as described previously (Li et al., 2014, 2018). qPCR conditions and primers are listed in Supplemental Information.

SUPPLEMENTAL INFORMATION

Supplemental Information can be found online at https://doi.org/10.1016/j.stemcr.2020.03.021.

AUTHOR CONTRIBUTIONS

H.J.-C. and Y.T.I. conceived the project and designed the experiments. H.J.-C., Q.L., and N.K.N. carried out the experiments. H.J.-C. and Y.T.I. wrote the manuscript and all authors amended the manuscript.

ACKNOWLEDGMENTS

We thank the Bloomington Drosophila Stock Center and Vienna Drosophila Resource Center for RNAi lines and stocks. Monoclonal

antibodies listed as DSHB were obtained from the Developmental Studies Hybridoma Bank, created by the NICHD of the NIH and maintained at The University of Iowa, Department of Biology, Iowa City, IA 52242. We thank Steven Hou, Jin Jiang, Huaqi Jiang, Hervé Agaisse, DJ Pan, Lei Zhang, Norbert Perrimon, and Andreas Bergmann for *Drosophila* stocks and reagents. This work was supported by NIH grants DK083450 and GM107457. Y.T.I. is a member of the UMass Center for Clinical and Translational Science (UL1TR000161).

Received: March 15, 2019
Revised: March 24, 2020
Accepted: March 25, 2020
Published: April 23, 2020

REFERENCES

Akagi, K., Wilson, K.A., Katewa, S.D., Ortega, M., Simons, J., Hilsabeck, T.A., Kapuria, S., Sharma, A., Jasper, H., and Kapahi, P. (2018). Dietary restriction improves intestinal cellular fitness to enhance gut barrier function and lifespan in *D. melanogaster*. PLos Genet. *14*, e1007777.

Amcheslavsky, A., Jiang, J., and Ip, Y.T. (2009). Tissue damage-induced intestinal stem cell division in *Drosophila*. Cell Stem Cell *4*, 49–61.

Antonello, Z.A., Reiff, T., Ballesta-Illan, E., and Dominguez, M. (2015). Robust intestinal homeostasis relies on cellular plasticity in enteroblasts mediated by miR-8-Escargot switch. EMBO J. *34*, 2025–2041.

Biteau, B., and Jasper, H. (2011). EGF signaling regulates the proliferation of intestinal stem cells in *Drosophila*. Development *138*, 1045–1055.

Boggiano, J.C., and Fehon, R.G. (2012). Growth control by committee: intercellular junctions, cell polarity, and the cytoskeleton regulate Hippo signaling. Dev. Cell *22*, 695–702.

Chakrabarti, S., Dudzic, J.P., Li, X., Collas, E.J., Boquete, J.P., and Lemaitre, B. (2016). Remote control of intestinal stem cell activity by haemocytes in *Drosophila*. PLoS Genet. *12*, e1006089.

Chen, J., Xu, N., Wang, C., Huang, P., Huang, H., Jin, Z., Yu, Z., Cai, T., Jiao, R., and Xi, R. (2018). Transient Scute activation via a self-stimulatory loop directs enteroendocrine cell pair specification from self-renewing intestinal stem cells. Nat. Cell Biol. *20*, 152–161.

Clark, R.I., and Walker, D.W. (2018). Role of gut microbiota in aging-related health decline: insights from invertebrate models. Cell Mol. Life Sci. *75*, 93–101.

Clevers, H., Loh, K.M., and Nusse, R. (2014). Stem cell signaling. An integral program for tissue renewal and regeneration: Wnt signaling and stem cell control. Science *346*, 1248012.

Cordero, J.B., Stefanatos, R.K., Scopelliti, A., Vidal, M., and Sansom, O.J. (2012). Inducible progenitor-derived Wingless regulates adult midgut regeneration in *Drosophila*. EMBO J. *31*, 3901–3917.

Dai, X., She, P., Chi, F., Feng, Y., Liu, H., Jin, D., Zhao, Y., Guo, X., Jiang, D., Guan, K.L., et al. (2013). Phosphorylation of angiomotin by Lats1/2 kinases inhibits F-actin binding, cell migration, and angiogenesis. J. Biol. Chem. *288*, 34041–34051.

Doupe, D.P., Marshall, O.J., Dayton, H., Brand, A.H., and Perrimon, N. (2018). *Drosophila* intestinal stem and progenitor cells are major sources and regulators of homeostatic niche signals. Proc. Natl. Acad. Sci. U S A *115*, 12218–12223.

Fletcher, G.C., Diaz-de-la-Loza, M.D., Borreguero-Munoz, N., Holder, M., Aguilar-Aragon, M., and Thompson, B.J. (2018). Mechanical strain regulates the Hippo pathway in *Drosophila*. Development *145*. https://doi.org/10.1242/dev.159467.

Furuse, M., and Izumi, Y. (2017). Molecular dissection of smooth septate junctions: understanding their roles in arthropod physiology. Ann. N. Y Acad. Sci. *1397*, 17–24.

Garcia-Hernandez, V., Quiros, M., and Nusrat, A. (2017). Intestinal epithelial claudins: expression and regulation in homeostasis and inflammation. Ann. N. Y Acad. Sci. *1397*, 66–79.

Guo, Z., and Ohlstein, B. (2015). Stem cell regulation. Bidirectional Notch signaling regulates *Drosophila* intestinal stem cell multipotency. Science *350*. https://doi.org/10.1126/science.aab0988.

Han, H., Qi, R., Zhou, J.J., Ta, A.P., Yang, B., Nakaoka, H.J., Seo, G., Guan, K.L., Luo, R., and Wang, W. (2018). Regulation of the Hippo pathway by phosphatidic acid-mediated lipid-protein interaction. Mol. Cell *72*, 328–340.e8.

Harden, N., Wang, S.J., and Krieger, C. (2016). Making the connection—shared molecular machinery and evolutionary links underlie the formation and plasticity of occluding junctions and synapses. J. Cell Sci. *129*, 3067–3076.

Herrera, S.C., and Bach, E.A. (2019). JAK/STAT signaling in stem cells and regeneration: from *Drosophila* to vertebrates. Development *146*. https://doi.org/10.1242/dev.167643.

Houtz, P., Bonfini, A., Liu, X., Revah, J., Guillou, A., Poidevin, M., Hens, K., Huang, H.Y., Deplancke, B., Tsai, Y.C., et al. (2017). Hippo, TGF-beta, and Src-MAPK pathways regulate transcription of the upd3 cytokine in *Drosophila* enterocytes upon bacterial infection. PLoS Genet. *13*, e1007091.

Izumi, Y., Furuse, K., and Furuse, M. (2019). Septate junctions regulate gut homeostasis through regulation of stem cell proliferation and enterocyte behavior in *Drosophila*. J. Cell Sci. *132*.

Izumi, Y., Motoishi, M., Furuse, K., and Furuse, M. (2016). A tetraspanin regulates septate junction formation in *Drosophila* midgut. J. Cell Sci. *129*, 1155–1164.

Izumi, Y., Yanagihashi, Y., and Furuse, M. (2012). A novel protein complex, Mesh-Ssk, is required for septate junction formation in the *Drosophila* midgut. J. Cell Sci. *125*, 4923–4933.

Jiang, H., Patel, P.H., Kohlmaier, A., Grenley, M.O., McEwen, D.G., and Edgar, B.A. (2009). Cytokine/Jak/Stat signaling mediates regeneration and homeostasis in the *Drosophila* midgut. Cell *137*, 1343–1355.

Karpowicz, P., Perez, J., and Perrimon, N. (2010). The Hippo tumor suppressor pathway regulates intestinal stem cell regeneration. Development *137*, 4135–4145.

Kwon, Y., Song, W., Droujinine, I.A., Hu, Y., Asara, J.M., and Perrimon, N. (2015). Systemic organ wasting induced by localized expression of the secreted insulin/IGF antagonist ImpL2. Dev. Cell *33*, 36–46.

Kwon, Y., Vinayagam, A., Sun, X., Dephoure, N., Gygi, S.P., Hong, P., and Perrimon, N. (2013). The Hippo signaling pathway interactome. Science *342*, 737–740.

Lee, T., and Luo, L. (2001). Mosaic analysis with a repressible cell marker (MARCM) for *Drosophila* neural development. Trends Neurosci. *24*, 251–254.

Li, Q., Li, S., Mana-Capelli, S., Roth Flach, R.J., Danai, L.V., Amcheslavsky, A., Nie, Y., Kaneko, S., Yao, X., Chen, X., et al. (2014). The conserved misshapen-warts-Yorkie pathway acts in enteroblasts to regulate intestinal stem cells in *Drosophila*. Dev. Cell *31*, 291–304.

Li, Q., Nirala, N.K., Nie, Y., Chen, H.J., Ostroff, G., Mao, J., Wang, Q., Xu, L., and Ip, Y.T. (2018). Ingestion of food particles regulates the mechanosensing misshapen-Yorkie pathway in *Drosophila* intestinal growth. Dev. Cell *45*, 433–449 e436.

Li, S., Cho, Y.S., Yue, T., Ip, Y.T., and Jiang, J. (2015). Overlapping functions of the MAP4K family kinases Hppy and Msn in Hippo signaling. Cell Discov. *1*, 15038.

Ma, S., Meng, Z., Chen, R., and Guan, K.L. (2018). The Hippo pathway: biology and pathophysiology. Annu. Rev. Biochem. *88*, 577–604.

Mana-Capelli, S., and McCollum, D. (2018). Angiomotins stimulate LATS kinase autophosphorylation and act as scaffolds that promote Hippo signaling. J. Biol. Chem. *293*, 18230–18241.

Mana-Capelli, S., Paramasivam, M., Dutta, S., and McCollum, D. (2014). Angiomotins link F-actin architecture to Hippo pathway signaling. Mol. Biol. Cell *25*, 1676–1685.

Meng, Z., Moroishi, T., Mottier-Pavie, V., Plouffe, S.W., Hansen, C.G., Hong, A.W., Park, H.W., Mo, J.S., Lu, W., Lu, S., et al. (2015). MAP4K family kinases act in parallel to MST1/2 to activate LATS1/2 in the Hippo pathway. Nat. Commun. *6*, 8357.

Meng, Z., Qiu, Y., Lin, K.C., Kumar, A., Placone, J.K., Fang, C., Wang, K.C., Lu, S., Pan, M., Hong, A.W., et al. (2018). RAP2 mediates mechanoresponses of the Hippo pathway. Nature *560*, 655–660.

Micchelli, C.A., and Perrimon, N. (2006). Evidence that stem cells reside in the adult *Drosophila* midgut epithelium. Nature *439*, 475–479.

Misra, J.R., and Irvine, K.D. (2018). The Hippo signaling network and its biological functions. Annu. Rev. Genet. *52*, 65–87.

Ohlstein, B., and Spradling, A. (2006). The adult *Drosophila* posterior midgut is maintained by pluripotent stem cells. Nature *439*, 470–474.

Ohlstein, B., and Spradling, A. (2007). Multipotent *Drosophila* intestinal stem cells specify daughter cell fates by differential notch signaling. Science *315*, 988–992.

Poon, C.L.C., Liu, W., Song, Y., Gomez, M., Kulaberoglu, Y., Zhang, X., Xu, W., Veraksa, A., Hergovich, A., Ghabrial, A., et al. (2018). A hippo-like signaling pathway controls tracheal morphogenesis in *Drosophila* melanogaster. Dev. Cell *47*, 564–575.e5.

Qin, Y., and Zhang, C. (2017). The regulatory role of IFN-gamma on the proliferation and differentiation of hematopoietic stem and progenitor cells. Stem Cell Rev *13*, 705–712.

Ren, F., Wang, B., Yue, T., Yun, E.Y., Ip, Y.T., and Jiang, J. (2010). Hippo signaling regulates *Drosophila* intestine stem cell proliferation through multiple pathways. Proc. Natl. Acad. Sci. U S A *107*, 21064–21069.

Rera, M., Clark, R.I., and Walker, D.W. (2012). Intestinal barrier dysfunction links metabolic and inflammatory markers of aging to death in *Drosophila*. Proc. Natl. Acad. Sci. U S A *109*, 21528–21533.

Resende, L.P., Truong, M.E., Gomez, A., and Jones, D.L. (2017). Intestinal stem cell ablation reveals differential requirements for survival in response to chemical challenge. Dev. Biol. *424*, 10–17.

Resnik-Docampo, M., Koehler, C.L., Clark, R.I., Schinaman, J.M., Sauer, V., Wong, D.M., Lewis, S., D'Alterio, C., Walker, D.W., and Jones, D.L. (2017). Tricellular junctions regulate intestinal stem cell behaviour to maintain homeostasis. Nat. Cell Biol. *19*, 52–59.

Resnik-Docampo, M., Sauer, V., Schinaman, J.M., Clark, R.I., Walker, D.W., and Jones, D.L. (2018). Keeping it tight: the relationship between bacterial dysbiosis, septate junctions, and the intestinal barrier in *Drosophila*. Fly (Austin) *12*, 34–40.

Salazar, A.M., Resnik-Docampo, M., Ulgherait, M., Clark, R.I., Shirasu-Hiza, M., Jones, D.L., and Walker, D.W. (2018). Intestinal Snakeskin limits microbial dysbiosis during aging and promotes longevity. iScience *9*, 229–243.

Shaw, R.L., Kohlmaier, A., Polesello, C., Veelken, C., Edgar, B.A., and Tapon, N. (2010). The Hippo pathway regulates intestinal stem cell proliferation during *Drosophila* adult midgut regeneration. Development *137*, 4147–4158.

Staley, B.K., and Irvine, K.D. (2010). Warts and Yorkie mediate intestinal regeneration by influencing stem cell proliferation. Curr. Biol. *20*, 1580–1587.

Su, T., Ludwig, M.Z., Xu, J., and Fehon, R.G. (2017). Kibra and merlin activate the Hippo pathway spatially distinct from and independent of expanded. Dev. Cell *40*, 478–490.e3.

Tian, A., and Jiang, J. (2014). Intestinal epithelium-drived BMP controls stem cell self-renewal in *Drosophila* adult midgut. eLife *3*, e01857.

Vancamelbeke, M., and Vermeire, S. (2017). The intestinal barrier: a fundamental role in health and disease. Expert Rev. Gastroenterol. Hepatol. *11*, 821–834.

Xu, C., Tang, H.W., Hung, R.J., Hu, Y., Ni, X., Housden, B.E., and Perrimon, N. (2019). The septate junction protein Tsp2A restricts intestinal stem cell activity via endocytic regulation of aPKC and Hippo signaling. Cell Rep. *26*, 670–688 e676.

Xu, N., Wang, S.Q., Tan, D., Gao, Y., Lin, G., and Xi, R. (2011). EGFR, Wingless and JAK/STAT signaling cooperatively maintain *Drosophila* intestinal stem cells. Dev. Biol. *354*, 31–43.

Yanagihashi, Y., Usui, T., Izumi, Y., Yonemura, S., Sumida, M., Tsukita, S., Uemura, T., and Furuse, M. (2012). Snakeskin, a membrane protein associated with smooth septate junctions, is required for intestinal barrier function in *Drosophila*. J. Cell Sci. *125*, 1980–1990.

Yu, J., and Pan, D. (2018). Validating upstream regulators of Yorkie activity in Hippo signaling through scalloped-based genetic epistasis. Development *145*. https://doi.org/10.1242/dev.157545.

Zeng, X., and Hou, S.X. (2015). Enteroendocrine cells are generated from stem cells through a distinct progenitor in the adult *Drosophila* posterior midgut. Development *142*, 644–653.

Zhao, B., Li, L., Lu, Q., Wang, L.H., Liu, C.Y., Lei, Q., and Guan, K.L. (2011). Angiomotin is a novel Hippo pathway component that inhibits YAP oncoprotein. Genes Dev. *25*, 51–63.

Zheng, Y., Wang, W., Liu, B., Deng, H., Uster, E., and Pan, D. (2015). Identification of happyhour/MAP4K as alternative hpo/mst-like kinases in the Hippo kinase cascade. Dev. Cell *34*, 642–655.

Zhou, F., Rasmussen, A., Lee, S., and Agaisse, H. (2013). The UPD3 cytokine couples environmental challenge and intestinal stem cell division through modulation of JAK/STAT signaling in the stem cell microenvironment. Dev. Biol. *373*, 383–393.

Zwick, R.K., Ohlstein, B., and Klein, O.D. (2019). Intestinal renewal across the animal kingdom: comparing stem cell activity in mouse and *Drosophila*. Am. J. Physiol. Gastrointest. Liver Physiol. *316*, G313–G322.